Proceedings of FUELCELL2005
Third International Conference on Fuel Cell Science, Engineering and Technology
May 23-25, 2005, Ypsilanti, Michigan
Paper Number 74046

NUMERICAL SIMULATIONS OF GASEOUS MIXTURE FLOW IN POROUS ELECTRODES FOR PEM FUEL CELLS BY THE LATTICE BOLTZMANN METHOD

Pietro Asinari [a, *], Marco Coppo [a], Michael R. von Spakovsky [b], Bhavani V. Kasula [b]

[a] Energy Engineering Department, Politecnico di Torino
Corso Duca degli Abruzzi 24, Torino, Zip Code 10129, Italy
Emails: pietro.asinari@polito.it, marco.coppo@polito.it
[*] Corresponding author. Tel. +39-011-564-4413, Fax. +39-011-564-4499.

[b] Center for Energy Systems Research, Mechanical Engineering Department
Virginia Polytechnic Institute and State University (Virginia Tech)
Blacksburg, VA 24061, U.S.A.
Emails: vonspako@vt.edu, bvkasula@vt.edu

ABSTRACT

Throughout the last decade, a considerable amount of work has been carried out in order to obtain ever more refined models of proton exchange membrane (PEM) fuel cells. While many of the phenomena occurring in a fuel cell have been described with ever more complex models, the flow of gaseous mixtures in the porous electrodes has continued to be modeled with Darcy's law in order to take into account interactions with the solid structure and with Fick's law in order to take into account interactions among species.

Both of these laws derive from the macroscopic continuum approach, which essentially consists of applying some sort of homogenization technique which properly averages the underlying microscopic phenomena for producing measurable quantities. Unfortunately, these quantities in the porous electrodes of fuel cells are sometimes measurable only in principle. For this reason, this type of approach introduces uncertain macroscopic parameters which can significantly affect the numerical results.

This paper is part of an ongoing effort to address the problem following an alternative approach. The key idea is to numerically simulate the underlying microscopic phenomena in an effort to bring the mathematical description nearer to actual reality. In order to reach this goal, some recently developed mesoscopic tools appear to be very promising since the microscopic approach is in this particularly case partially included in the numerical method itself. In particular, the lattice Boltzmann models treat the problem by reproducing the collisions among particles of the same type, among particles belonging to different species, and finally among the species and the solid obstructions. Recently, a procedure based on a lattice Boltzmann model for calculating the hydraulic constant as a function of material structure and applied pressure gradient was defined and applied. This model has since been extended in order to include gaseous mixtures with different methods being considered in order to simulate the coupling strength among the species. The present paper reports the results of this extended model for PEM fuel cell applications and in particular for the analysis of the fluid flow of gaseous mixtures through porous electrodes. Because of the increasing computational needs due to both three–dimensional descriptions and multi-physics models, the need for large parallel computing is indicated and some features of this improvement are reported.

INTRODUCTION

Refined models of proton exchange membrane (PEM) fuel cells are important tools in order to further improve the design and performance of these devices. The mathematical models obtained were first numerically implemented in one dimension [1-6] whereas, recently, several research groups have produced detailed two- and three–dimensional models of this type of fuel cell [7-17]. Such models have helped considerably in understanding the complex phenomena occurring during fuel cell operation and have contributed to improved fuel cell designs.

However, all of this work was based on a macroscopic approach to fuel cell modeling. In other words, the actual micro structure of the porous layers that constitute a fuel cell was not modeled, and its effects on cell operation and performance were taken into account by considering homogeneous layers characterized by macroscopic, averaged parameters such as porosity and tortuosity.

While this eases the modeling efforts, it carries two disadvantages. Firstly, if an in–situ measurement of such macroscopic quantities is performed, the related uncertainties are bound to affect the model results, whereas if porosity and tortuosity are treated as fitting parameters, there is no guarantee that the true values are used since such parameters can be used to compensate for the inaccurate modeling of other phenomena. Secondly, it has been shown [18] that different porous layer micro structures, characterized by the same porosity, show different hydraulic characteristics. In other words, no macroscopic parameter can exhaustively describe what happens at microscopic levels.

In order to overcome these limitations, a novel approach to gas flow modeling in porous media, based on the lattice Boltzmann methods (LBMs), was utilized. LBMs are efficient numerical tools for investigating flow in highly complex geometries, such as porous media [19-21]. Even though traditional Navier-Stokes solvers could be used to describe porous media flow, LB methods do not require pressure-velocity decoupling or the resolution of a large system of algebraic equations [22, 23]. They solve a simplified Boltzmann equation for an ensemble-averaged distribution of moving, interacting particles on a discrete lattice. The macroscopic quantities that describe the fluid flow can be calculated as integrals of this distribution. Since the motion of particles is limited to fixed paths connecting lattice nodes, the resolution process needs only information about nearest neighbor nodes. This feature, along with the explicit nature of the numerical scheme, makes LBMs very suitable for parallelization.

The lattice Boltzmann models seem to be very promising for the analysis of reactive mixtures in porous catalyst layers [24, 25]. For this reason, a lot of work has been performed in recent years in order to produce reliable lattice Boltzmann models for multi-component fluids and, in particular, for mixtures composed of miscible species [26–30]. The problem is to find a proper way, within the framework of a simplified kinetic model, for describing the interactions among different particles. Once this milestone is achieved, the extension of the model to reactive flows is straightforward [31, 32] and essentially involves additional source terms in the species equations which result from the reaction rate. Unfortunately most existing lattice Boltzmann models for mixtures [26–32] are based on heuristic assumptions or prescribe too many constraints for setting the microscopic parameters, the end result of which is an idealized macroscopic description.

The aim of the present study is twofold. Firstly, the original non-reactive single species model developed by Asinari and Coppo (two of the present authors) [18] must be extended in order to deal with reactive gas mixtures, thus, enabling the simulation of fluid flow in a PEM fuel cell cathode catalyst layer. Secondly, a domain decomposition and code parallelization that could take advantage of the LBM characteristics in order to reduce computational times must be defined.

The ultimate goal of the present work is that of obtaining a complete mesoscopic model of fluid flow and reaction in three dimensional fuel cell porous media. The advantage of this would be that only the medium microstructure would need to be measured (for example by means of a tomography scan) and then cell performance could be predicted. The reduced computational times obtained with code parallelization and the reactive gas mixture LB model developed represent a concrete step towards the achievement of this goal.

MATHEMATICAL MODEL FOR REACTIVE MIXTURE FLOW IN POROUS MEDIA

Continuous kinetic model

Following the derivation of the Boltzmann equation for a simple system with a single species, the kinetic equations for a simple system comprised of a mixture can be derived in a very similar way [33–35]. Let us consider a mixture composed of only two types of particles labeled *a* and *b*. The two Boltzmann equations for the binary system are

$$\frac{\partial f_a}{\partial t} + \mathbf{v}\cdot\nabla f_a + \mathbf{g}_a\cdot\nabla_{\mathrm{v}} f_a = Q_{aa} + Q_{ab}\,, \tag{1}$$

$$\frac{\partial f_b}{\partial t} + \mathbf{v}\cdot\nabla f_b + \mathbf{g}_b\cdot\nabla_{\mathrm{v}} f_b = Q_{ba} + Q_{bb}\,, \tag{2}$$

where $f_a(\mathbf{x},\mathbf{v},t)$ is the continuous single particle distribution function for the *a* species, $\mathbf{v}$ is the microscopic velocity, $\mathbf{g}_a$ is the acceleration due to an external field for the *a* species, and similar definitions hold for the *b* species too. The quadratic expressions Q_{aa} and Q_{bb} are the collisional terms which describe the collisions among particles of the same type (*self-collisions*), while Q_{ab} and Q_{ba} are the collisional terms due to the interactions among different species (*cross-collisions*).

Each collision term has a well–known structure similar to the collision operator involved in the Boltzmann equation for a single fluid [18]. The time evolution of the distribution function for each species is affected both by collisions with particles of the same type and with particles of different type. These two phenomena are the kinetic driving forces of the equilibration process for the whole mixture.

A simplified kinetic model which allows one to separately describe both the driving forces, as they appear in the original Boltzmann equations, would be desirable. Essentially the key idea is to substitute the previous collisional terms with simplified ones, which are selected with a BGK–like structure. The model obtained is due to Hamel [36–38]. In the following, only the equation for a generic species $\sigma = a, b$ will be considered. The simplified kinetic equation has the general form

$$\frac{\partial f_\sigma}{\partial t} + \mathbf{v}\cdot\nabla f_\sigma + \mathbf{g}_\sigma\cdot\nabla_{\mathrm{v}} f_\sigma = -\frac{1}{\tau_\sigma}\left[f_\sigma - f_\sigma^e\right] - \frac{1}{\tau_m}\left[f_\sigma - f_{\sigma(m)}^e\right], \tag{3}$$

where τ_σ is the relaxation time constant for self-collisions, τ_m is the relaxation time constant for cross-collisions, f_σ^e is a Maxwellian distribution function centered on the specific velocity, while $f_{\sigma(m)}^e$ is a Maxwellian distribution function centered on a characteristic velocity for the mixture. The explicit expressions of these Maxwellians are

$$f_\sigma^e = \frac{\rho_\sigma / m_\sigma}{(2\pi e_\sigma)^{D/2}} exp\left[-\frac{1}{2}\frac{(\mathbf{v}-\mathbf{u}_\sigma)^2}{e_\sigma}\right], \tag{4}$$

$$f_{\sigma(m)}^e = \frac{\rho_\sigma / m_\sigma}{(2\pi e_\sigma)^{D/2}} exp\left[-\frac{1}{2}\frac{(\mathbf{v}-\mathbf{u})^2}{e_\sigma}\right], \tag{5}$$

where ρ_σ is the density, m_σ the particle mass, $\mathbf{u}_\sigma$ is the macroscopic velocity, $\mathbf{u}$ is the macroscopic barycentric velocity, e_σ is the internal energy, and D the number of physical dimensions. The barycentric velocity is defined as

$$\mathbf{u} = \sum_\sigma x_\sigma \mathbf{u}_\sigma = \sum_\sigma \rho_\sigma \mathbf{u}_\sigma / \sum_\sigma \rho_\sigma\,, \tag{6}$$

where x_σ is the mass concentration (mass fraction) for the generic species. Local momentum conservation implies that the relaxation time constant τ_m for the cross-collisions must be the same for all species.

Macroscopic quantities, such as the density $\rho_\sigma(\mathbf{x},t)$, the macroscopic specific velocity $\mathbf{u}_\sigma(\mathbf{x},t)$, and, consequently, the macroscopic barycentric velocity $\mathbf{u}(\mathbf{x},t)$ can be calculated as the moments of the density distribution function, i.e.

$$\rho_\sigma(\mathbf{x},t)=\int_{-\infty}^{+\infty} m_\sigma f_\sigma \, d\mathbf{v}\,, \tag{7}$$

$$\rho_\sigma \mathbf{u}_\sigma(\mathbf{x},t)=\int_{-\infty}^{+\infty} m_\sigma \mathbf{v} f_\sigma \, d\mathbf{v}\,. \tag{8}$$

Using the Chapman–Enskog procedure, a suitable expansion of certain solutions of equations (3) recovers the Navier–Stokes macroscopic description when the bulk viscosity is neglected [39], yielding

$$\frac{\partial \rho_\sigma}{\partial t}+\nabla\cdot(\rho_\sigma \mathbf{u}_\sigma)=0\,, \tag{9}$$

$$\begin{aligned}&\frac{\partial}{\partial t}(\rho_\sigma \mathbf{u}_\sigma)+\nabla(\rho_\sigma e_\sigma)-\rho_\sigma \mathbf{g}_\sigma+\rho_\sigma \mathbf{w}_\sigma/\tau_m\\ &\quad+\nabla\cdot\left[(1-\alpha_\sigma)\rho_\sigma \mathbf{u}_\sigma\otimes\mathbf{u}_\sigma+\alpha_\sigma\rho_\sigma \mathbf{u}\otimes\mathbf{u}\right.\\ &\quad\left.+\alpha_\sigma \rho_\sigma \mathbf{u}_{\alpha(\sigma)}\otimes\mathbf{w}_\sigma+\alpha_\sigma \rho_\sigma \mathbf{w}_\sigma\otimes\mathbf{u}_{\alpha(\sigma)}\right]=\\ &\quad+\nabla\cdot\left\{\alpha_\sigma \rho_\sigma e_\sigma \tau_m\left[\nabla\mathbf{u}_{\alpha(\sigma)}+\nabla\mathbf{u}_{\alpha(\sigma)}^T\right]\right\}\end{aligned}, \tag{10}$$

where $\alpha_\sigma=\tau_\sigma/(\tau_\sigma+\tau_m)$ is a bounded function of the relaxation time constants such that $0\le\alpha_\sigma\le 1$, $\mathbf{w}_\sigma=\mathbf{u}_\sigma-\mathbf{u}$ is the diffusion velocity with regard to the macroscopic barycentric velocity and $\mathbf{u}_{\alpha(\sigma)}=(1-\alpha_\sigma)\mathbf{u}_\sigma+\alpha_\sigma\mathbf{u}$ is a linear combination between the specific velocity and the macroscopic barycentric velocity. Unlike what happens at macroscopic level when the usual BGK equation is considered, in the Hamel model, the relaxation time constants affect the advection term, the viscous term, and an internal forcing term $\rho_\sigma \mathbf{w}_\sigma/\tau_m$, which directly allows the exchange of momentum among the species. In a mesoscopic framework, a strategy for setting the relaxation time constants of the model is needed.

Before proceeding in this direction, it is worth highlighting that the macroscopic equations which derive from the Hamel kinetic model do not involve chemical reactions, because there is no source term in the continuity equation. As will be discussed further, the discretization of the phase space will be performed on a suitable lattice. Since the number of discrete microscopic velocities should be as small as possible, some additional terms naturally arise from the discretization process and the macroscopic equations of the discrete model do not match perfectly those which derive from the continuous model. The majority of these spurious terms will be cancelled by properly designing the lattice and those which appear in the continuity equation will be used to match source terms due to chemical reactions.

Discrete kinetic model

To solve the continuous kinetic equation (equation (3)), the discrete ordinate method can be applied [40, 41]. According to this method, a set of discrete microscopic velocities $\mathbf{v}_i$ must be defined on which the distribution function is evaluated. The generic function $f_\sigma^i(\mathbf{x},t)$ is the single particle distribution function evaluated for velocity $\mathbf{v}_i$ at $(\mathbf{x},t)$. In the suggested model, a square lattice called D2Q9 for a two–dimensional computational domain, which makes use of nine discrete velocities, is considered [42]. This assumption simplifies the development of the numerical code, but it is nonessential for the physical model. Efforts aimed at extending the present numerical code in order to include a three–dimensional computational domain are currently under development. In particular, the number of discrete microscopic velocities needed for recovering the correct macroscopic equations in three–dimensional geometries is higher and can include as many as nineteen velocities (e.g., the D3Q19 lattice [42]).

The lattice discrete velocities for the two–dimensional case are defined in the following way:

$$v_i^x=\begin{cases}0 & i=0\\ c\cos[(i-1)\pi/2] & i=1,\ldots,4\\ c\sqrt{2}\cos[(i-9/2)\pi/2] & i=5,\ldots,8\end{cases}, \tag{11}$$

$$v_i^y=\begin{cases}0 & i=0\\ c\sin[(i-1)\pi/2] & i=1,\ldots,4\\ c\sqrt{2}\sin[(i-9/2)\pi/2] & i=5,\ldots,8\end{cases}, \tag{12}$$

where c is a tunable parameter which is called the lattice velocity. Thus, the kinetic equation, which is an integro-differential equation, reduces to a system of differential equations. Moreover, the term that takes into account the effect of the external force field can be simplified [43] such that

$$\begin{aligned}&\frac{\partial f_\sigma^i}{\partial t}+\mathbf{v}_i\cdot\nabla f_\sigma^i=-\frac{1}{\tau_\sigma}\left[f_\sigma^i-f_\sigma^{ei}\right]\\ &\quad-\frac{1}{\tau_m}\left[f_\sigma^i-f_{\sigma(m)}^{ei}\right]+(1-\alpha_\sigma)\frac{f_\sigma^{ei}}{e_\sigma}(\mathbf{v}_i-\mathbf{u}_\sigma)\cdot\mathbf{g}_\sigma\,.\\ &\quad+\alpha_\sigma\frac{f_{\sigma(m)}^{ei}}{e_\sigma}(\mathbf{v}_i-\mathbf{u})\cdot\mathbf{g}_\sigma\end{aligned} \tag{13}$$

Since only the distribution functions for discrete microscopic velocities are considered, an interpolation test function must be adopted to calculate the macroscopic quantities. In this way, the previous integrals (equations (7) and (8)) reduce to weighted summations of the considered discrete functions. The interpolation test function should be as similar to the Maxwellian distribution function as possible in order to easily include the equilibrium conditions. If we consider the regime of low speed fluid motion ($|\mathbf{u}_\sigma|\ll|\mathbf{v}|$), which essentially means $|\mathbf{u}_\sigma|\ll c$, both equilibrium distribution functions can be linearized around the state at rest [41], namely, $f_\sigma^{e,i}\cong K_\sigma^i\varphi_\sigma^{e,i}$ and $f_{\sigma(m)}^{e,i}\cong K_\sigma^i\varphi_{\sigma(m)}^{e,i}$ where

$$K_\sigma^i=\frac{1}{m_\sigma(2\pi e_\sigma)^{D/2}}exp\left(-\frac{1}{2}\frac{\mathbf{v}_i^2}{e_\sigma}\right), \tag{14}$$

$$\varphi_\sigma^{e,i}=\rho_\sigma\left[1+\frac{\mathbf{v}_i\cdot\mathbf{u}_\sigma}{e_\sigma}+\frac{1}{2}\left(\frac{\mathbf{v}_i\cdot\mathbf{u}_\sigma}{e_\sigma}\right)^2-\frac{1}{2}\frac{\mathbf{u}_\sigma^2}{e_\sigma}\right], \tag{15}$$

and a similar expression holds for $\varphi_{\sigma(m)}^{e,i}$ but centered on the macroscopic barycentric velocity. Since the deviation of the distribution function from the one at rest is also small, it is assumed that the function $\varphi_\sigma^i=f_\sigma^i/K_\sigma^i$ can be approximated by an interpolation test function, which is a D-dimensional

polynomial of second order as is that for the function $\varphi_\sigma^{e,i}$ precisely. The modified distribution functions for the discrete microscopic velocities, φ_σ^i, satisfy a system of differential equations similar to the original one for the discretized distribution functions.

Since only terms up to second order for the macroscopic quantities have been considered in the previous approximations, the forcing terms in the kinetic equations which define the discrete model can be simplified, namely,

$$\begin{aligned}\frac{\partial \varphi_\sigma^i}{\partial t}+\mathbf{v}_i\cdot\nabla\varphi_\sigma^i &= -\frac{1}{\tau_\sigma}\left[\varphi_\sigma^i-\varphi_\sigma^{ei}\right]\\ &-\frac{1}{\tau_m}\left[\varphi_\sigma^i-\varphi_{\sigma(m)}^{ei}\right]+\frac{1}{\sqrt{e_\sigma}}\mathbf{k}_{\alpha(\sigma)}^i\cdot\mathbf{g}_\sigma\end{aligned}, \tag{16}$$

where

$$\mathbf{k}_{\alpha(\sigma)}^i=\rho_\sigma\left[\frac{\mathbf{v}_i-\mathbf{u}_{\alpha(\sigma)}}{\sqrt{e_\sigma}}+\frac{\mathbf{v}_i\cdot\mathbf{u}_{\alpha(\sigma)}}{\sqrt{e_\sigma^3}}\mathbf{v}_i\right]. \tag{17}$$

The left hand side of equation (16) is essentially a substantial derivative and involves a known microscopic velocity of the lattice. For this reason, the method of characteristics (MOC) can easily be applied for reducing the system of partial differential equations to a system of ordinary differential equations by moving along the characteristic surfaces defined by the following expression $\mathbf{x}_i^c=\mathbf{v}_i(t-t_0)+\mathbf{x}_0$. The ordinary derivatives can be numerically estimated by considering the rate of change of a finite time step δt smaller than the characteristic time scales of the phenomena. The spurious terms, which derive from the previous approximation at the hydrodynamic level, are called discrete lattice effects. In order to cancel the discrete lattice effects, some corrections are need.

Let us define the following corrected moments:

$$\rho_\sigma(\mathbf{x},t)=\sum_i\varsigma_i\varphi_\sigma^i, \tag{18}$$

$$\begin{aligned}\rho_\sigma\mathbf{u}_\sigma^\oplus(\mathbf{x},t)=\sum_k\Bigg[&\left(\frac{2}{2+\delta t/\tau_m}\delta_{k\sigma}\right.\\ &\left.+\frac{\delta t/\tau_m}{2+\delta t/\tau_m}x_k\right)\left(\sum_i\varsigma_i\,\mathbf{v}\varphi_\sigma^i+\rho_\sigma\mathbf{g}_k\,\delta t/2\right)\Bigg],\end{aligned} \tag{19}$$

where $\delta_{k\sigma}=1$ if $k=\sigma$ and $\delta_{k\sigma}=0$ otherwise, while the weight factors involved in the quadrature formulas are defined in the following way:

$$\varsigma_i=\begin{cases}4/9 & i=0\\ 1/9 & i=1,...,4\\ 1/36 & i=5,...,8\end{cases}. \tag{20}$$

It is worth highlighting that the usual definitions are recovered when the discrete lattice effects can be neglected, i.e. when a very fine lattice is considered ($\delta t\to 0$). In the last case, the corrected velocity is equal to the conventional one $\mathbf{u}_\sigma^\oplus\to\mathbf{u}_\sigma$.

In a similar fashion, the discrete kinetic equations must be modified too. At this stage, a small correction in order to include source terms in the continuity equations has been added because the analysis of reactive flows is the final goal of the present paper. This yields

$$\begin{aligned}\varphi_\sigma^i(t+\delta t,\mathbf{x}+\mathbf{v}_i\,\delta t)-\varphi_\sigma^i(t,\mathbf{x})&=\delta t\,S_\sigma\\ -\frac{\delta t}{\tau_\sigma}\left[\varphi_\sigma^i-\varphi_\sigma^{ei\oplus}\right]-\frac{\delta t}{\tau_m}&\left[\varphi_\sigma^i-\varphi_{\sigma(m)}^{ei\oplus}\right]\\ +\frac{\delta t}{\sqrt{e_\sigma}}\mathbf{k}_{\alpha(\sigma)}^i&\cdot\left[d_\sigma\mathbf{g}_\sigma+(1-d_\sigma)\mathbf{w}_\sigma^\oplus/\tau_m\right]\end{aligned}, \tag{21}$$

where S_σ is the generic source term in the continuity equation and d_σ is the discrete factor defined as

$$d_\sigma=1-\frac{\delta t}{2}\left(\frac{1}{\tau_\sigma}+\frac{1}{\tau_m}\right). \tag{22}$$

It is possible to recover equation (16) by neglecting the chemical reactions ($S_\sigma=0$), considering a very fine lattice ($\delta t\to 0$), and, consequently, neglecting the discrete lattice effects ($d_\sigma\to 1$).

A Chapman–Enskog procedure is again applied to derive the macroscopic equations of the corrected model [39], namely,

$$\frac{\partial\rho_\sigma}{\partial t}+\nabla\cdot(\rho_\sigma\mathbf{u}_\sigma^\oplus)=S_\sigma, \tag{23}$$

$$\begin{aligned}&\frac{\partial}{\partial t}(\rho_\sigma\mathbf{u}_\sigma^\oplus)+\nabla(\rho_\sigma e_\sigma)-\rho_\sigma\mathbf{g}_\sigma+\rho_\sigma\mathbf{w}_\sigma^\oplus/\tau_m\\ &+\nabla\cdot\Big[(1-\alpha_\sigma)\rho_\sigma\mathbf{u}_\sigma^\oplus\otimes\mathbf{u}_\sigma^\oplus+\alpha_\sigma\rho_\sigma\mathbf{u}^\oplus\otimes\mathbf{u}^\oplus\\ &+\alpha_\sigma\rho_\sigma\mathbf{u}_{\alpha(\sigma)}^\oplus\otimes\mathbf{w}_\sigma^\oplus+\alpha_\sigma\rho_\sigma\mathbf{w}_\sigma^\oplus\otimes\mathbf{u}_{\alpha(\sigma)}^\oplus\Big]=\\ &+\nabla\cdot\left\{d_\sigma\alpha_\sigma\rho_\sigma e_\sigma\tau_m\left[\nabla\mathbf{u}_{\alpha(\sigma)}^\oplus+(\nabla\mathbf{u}_{\alpha(\sigma)}^\oplus)^T\right]\right\}\end{aligned}. \tag{24}$$

In the derivation of equation (24), it has been assumed that $\rho_\sigma\gg\delta t\,S_\sigma$ because the discretization time step is usually small enough. This allows one to neglect the effects due to the term $\delta t\,S_\sigma$ in the pressure gradient involved in the macroscopic momentum equation.

Essentially, the macroscopic equations derived from the discrete kinetic model are very similar to those derived from the continuous Hamel model. However, the former allow one to consider chemical reactions and are formulated in terms of the corrected velocity $\mathbf{u}_\sigma^\oplus$ instead of the usual velocity $\mathbf{u}_\sigma$. Furthermore, the viscosity of the discrete equations (last term in the momentum equation (equation (24))) involves an additional factor which is d_σ. Both these differences are not significant and they can be properly compensated for by the mesoscopic tuning strategy. The previous equations are valid only if the low speed limit $|\mathbf{u}_\sigma|\ll c$ is satisfied.

The macroscopic equations for the discrete model (equations (23) and (24)) do not directly recover the Navier–Stokes model. A mesoscopic tuning strategy is needed which defines how to choose the microscopic relaxation times in order to recover the desired macroscopic transport coefficients.

Mesoscopic tuning strategy

Let us first consider the ideally, non–interacting configuration, i.e. when $1/\tau_m \to 0$. Let us define $\omega_\sigma^0 = \delta t^0 / \tau_\sigma^0$ as the dimensionless frequency for the generic component and c_σ^0 as the lattice velocity for the generic component. Since the dimensionless frequency must be set in such a way as to respect the stability criterion $0 \le \omega_\sigma^0 \le 2$, the problem becomes one of defining c_σ^0 and τ_σ^0 in order to recover the desired lattice grid size δx and the kinematic viscosity for the single component ν_σ. Thus, one arrives at

$$\tau_\sigma^0 = \frac{2-\omega_\sigma^0}{6(\omega_\sigma^0)^2}\frac{\delta x^2}{\nu_\sigma}, \tag{25}$$

$$c_\sigma^0 = \frac{6\,\omega_\sigma^0}{2-\omega_\sigma^0}\frac{\nu_\sigma}{\delta x}. \tag{26}$$

Since all the mixture components are computed on the same lattice, the lattice velocities must all be identical, i.e. $c_\sigma^0 = c^0$. This introduces a new constraint for the dimensionless frequencies. Let us label with *s* the component of the mixture characterized by the smallest viscosity: in this way $\nu_\sigma^0 \ge \nu_s^0$. The condition $c_\sigma^0 = c^0$ implies then that

$$\omega_\sigma^0 = \frac{2\nu_a\,\omega_s^0}{\nu_\sigma(2-\omega_s^0)+\nu_s\,\omega_s^0} \le \omega_s^0. \tag{27}$$

If ω_s^0 is selected in such a way that $0 \le \omega_s^0 \le 2$, then all the other dimensionless frequencies will follow the previous condition; and they will satisfy $0 \le \omega_\sigma^0 \le 2$ too. In particular, the previous condition implies that the discretization time steps for all the components will be identical to $\delta t^0 = \tau_\sigma^0\omega_\sigma^0 = \tau_s^0\omega_s^0$.

We can proceed in a similar fashion for the ideally, miscible configuration. Let us define $\omega_m^0 = \delta t^0 / \tau_m^0$ as the dimensionless frequency for the ideally miscible configuration. In this case, the problem is to define c_m^0 and τ_m^0 so as to recover the kinematic mixture viscosity ν_m. In this case, one arrives at

$$\tau_m^0 = \frac{2-\omega_m^0}{6(\omega_m^0)^2}\frac{\delta x^2}{\nu_m}, \tag{28}$$

$$c_m^0 = \frac{6\,\omega_m^0}{2-\omega_m^0}\frac{\nu_m}{\delta x}. \tag{29}$$

In this case, the lattice velocities are naturally identical, and the discretization time step is $\delta t^m = \tau_m^0\omega_m^0$.

For an intermediate configuration, i.e. moderate mixing, a generalized expression for the discretization time step can be assumed, namely,

$$\delta t = \lambda\,\delta t^0 + \varepsilon\,\delta t^m = \lambda\,\tau_s^0\omega_s^0 + \varepsilon\,\tau_m^0\omega_m^0, \tag{30}$$

where $\lambda = \tau_\sigma / \tau_\sigma^0$ and $\varepsilon = \tau_m / \tau_m^0$ are bounded interpolation parameters such that $0 \le \lambda$ and $\varepsilon \le 1$. The parameter ε can be set by means of experimental data on the diffusion coefficient for weakly interacting components. The parameter λ can be set in order to recover the effective mixture viscosity ν_m^e for the barycentric momentum equation, which essentially affects the value of the average macroscopic barycentric velocity throughout the porous medium [39].

NUMERICAL IMPLEMENTATION

Algorithm

A numerical code which implements the lattice Boltzmann scheme discussed in the previous sections was developed. A brief description of the main characteristics of the code is reported here.

In the following calculations, both the BGK–like collision operators are assumed constant during each time step. This assumption introduces a second–order truncation error, but the only effect is a change of the effective viscosity for the generic species and the need of considering a modified velocity. The main advantage of this is the possibility to decouple the resolution of the BGK–like equations (21) into three easier steps, i.e. moment calculation step, collision step and streaming step. First of all, the *calculation step* aims to calculate the Maxwellian distribution functions for the corrected specific velocity $\varphi_\sigma^{ei\oplus}$ and for the corrected barycentric velocity $\varphi_{\sigma(m)}^{ei\oplus}$. During the *collision step*, the new discrete distribution functions are evaluated as follow:

$$\begin{aligned}\varphi_\sigma^{i\,\Theta}(t,\mathbf{x}) = {} & \delta t\, S_\sigma \\ & -\frac{\delta t}{\tau_\sigma}\left[\varphi_\sigma^i - \varphi_\sigma^{ei\oplus}\right] - \frac{\delta t}{\tau_m}\left[\varphi_\sigma^i - \varphi_{\sigma(m)}^{ei\oplus}\right] \\ & +\frac{\delta t}{\sqrt{e_\sigma}}\mathbf{k}_{\alpha(\sigma)}^i \cdot \left[d_\sigma\,\mathbf{g}_\sigma + (1-d_\sigma)\mathbf{w}_\sigma^\oplus / \tau_m\right]\end{aligned}. \tag{31}$$

Finally during the *streaming step*, the new discrete distribution functions are properly assigned to the correct spatial locations, i.e.

$$\varphi_\sigma^i(t+\delta t, \mathbf{x}+\mathbf{v}_i\,\delta t) = \varphi_\sigma^{i\Theta}(t,\mathbf{x}). \tag{32}$$

A proper set of boundary conditions must be considered [44, 45]. Since the computational domain is chosen to be smaller than the physical thickness of the cathode catalyst layer, periodic geometric conditions are considered. This means that it must be imagined that the computational domain shown in the following figures must be repeated in both directions an infinite number of times in order to create the actual topology of the cathode catalyst layer. Unfortunately, in this case, the same trick can not be applied for the boundary conditions as well. In fact the chemical reactions modify the mass flow rate of the generic species, while periodic boundary conditions imply the same mass flow rate in each subdomain. For this reason, the actual boundary conditions are set in two steps. In the first step, some fluid cells at the boundary of the computational domain are selected as inlet ports and some others as outlet ports, according to the results of a preliminary calculation based on periodic boundary conditions and no chemical reactions. In the second step, for the inlet ports, a Maxwellian distribution function is adopted in order to impose the desired inlet

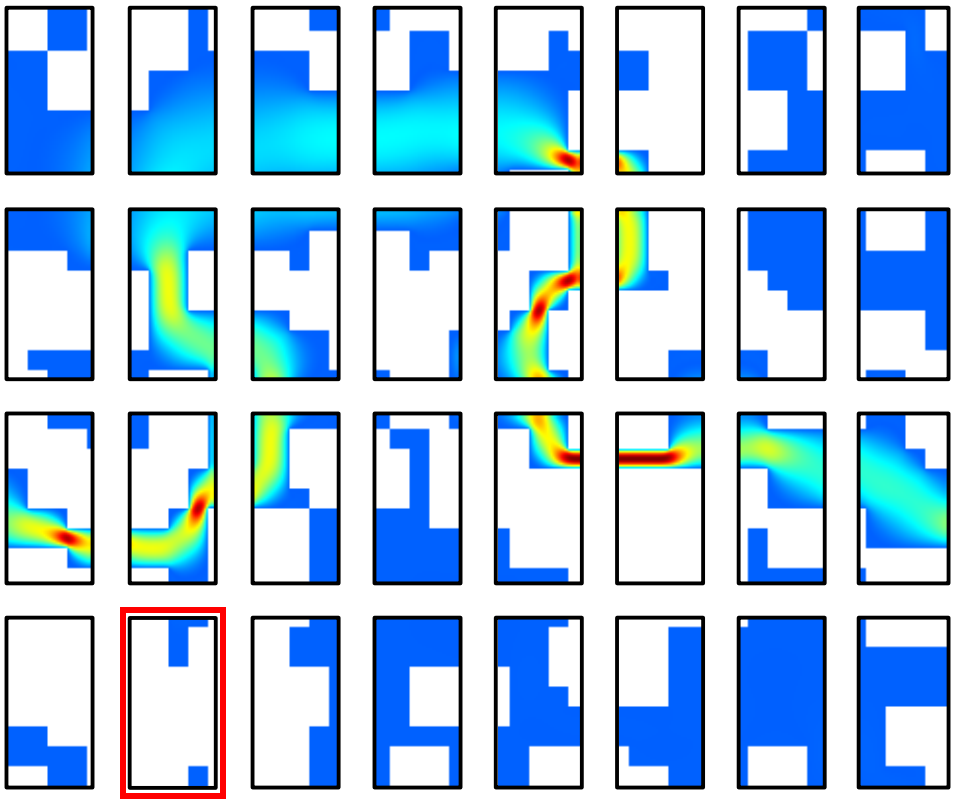

Figure 1. Elementary decomposition strategy for a parallel calculation based on 32 nodes. The highlighted subdomain is characterized by smaller porosity than the average one for the whole porous medium, and this leads to unbalanced calculations.

velocity and concentration. For the outlet ports an extrapolation scheme is used [45], which essentially involves the information inside the computational domain in order to estimate the distribution function at the outlet ports. This practice is based on the assumption that downstream information does not affect the computational domain too much. Inside the domain, additional boundary conditions must be considered in order to ensure the no–slip condition at the walls. In the present calculation, the no–slip boundary conditions are applied by default, but a check is introduced for the local Knudsen number, which allows one to switch to slip flow where necessary.

The calculation of reactive mixture flow in porous media can be quite demanding in terms of computational resources. Parallel computing is a useful tool for reducing the computational time and increasing the number of simulations to a reasonable value. Some details about parallel computing and the preliminary performance of the code developed are reported in the next section. Here, the focus is on how the parallelization modifies the algorithm of the numerical code.

Essentially, the numerical code developed can be divided into two main parts: the pre–processing task and the calculation task. The calculation task is made up of a number of operations which are performed at each time step.

- ***Pre-processing Task.*** The microscopic lattice parameters are calculated according to the mesoscopic tuning strategy in order to match the user input data for the macroscopic transport coefficients. The computational domain is divided into smaller portions according to the decomposition strategy and each one of them is sent to a node of the cluster (see Fig. 1). At this point, all the nodes of the cluster will perform the same operation on their subdomain under the co–ordination of a special node called the master node. Each computational subdomain is locally discretized by a given number of nodes in order to produce reliable mesh–independent results (local grid refinement).

- ***Calculation Task.*** The calculation can be divided into five phases.

  1. ***Collision.*** Both discrete Maxwellian equilibrium distribution functions are evaluated by using the macroscopic quantities for the generic species and for the mixture. The new values for each discrete velocity are calculated and stored.
  2. ***Communications.*** Each node sends the boundary values of the discrete distribution functions to the corresponding nodes which are adjacent to the one considered in the global computational domain. All the nodes must be synchronized before proceeding to the streaming step.
  3. ***Streaming.*** The discrete distribution functions are updated by moving them according to the generic direction of the allowed lattice set.
  4. ***Boundary conditions.*** All values of the unknown discrete distribution functions for the inward–pointing links are evaluated. For links that refer to nodes out of the computational domain, Maxwellian distribution functions (inlet ports) or extrapolated data (outlet ports) are applied.
  5. ***Moments.*** The corrected macroscopic quantities, which are moments of the distribution function, are evaluated.

In the following computations, a mesh–independent solution is found when the results for the default mesh and finer mesh differ by less than 2 %.

Parallelization

In this section, some preliminary features of the parallel lattice Boltzmann code which is currently under development are discussed. The reported numerical results were obtained on a Virginia Tech (VT) cluster facility, which is essentially a 200 node Myrinet/switched Ethernet cluster called ANANTHAM[1]. The code has been developed in C++ and a free communication library has been adopted (MPICH 1.3) based on MPI technology [46].

Before proceeding with the analysis of the parallel code, let us introduce some useful concepts:

- N [-], the number of nodes involved in the parallel calculation considered;
- WT_N [s], the wall clock time, which is the real physical time perceived by the final user;
- $CT_N = WT_N \cdot N$ [s], the CPU time which describes the calculation load for the cluster;
- CT_N^P [s], the pre–processing CPU time which describes the calculation load for the cluster due to the pre–processing task;
- CT_N^C [s], the calculation CPU time which describes the calculation load for the cluster due to actual calculations;
- $SpUp_N = WT_1 / CT_N$ [-], the speed–up efficiency which essentially compares the wall clock time due to single–node calculations (WT_1) and the actual CPU time due to the simultaneous utilization of N computational nodes ($CT_N = WT_N \cdot N$).
- $1/SpUp_N = (CT_N^P + CT_N^C)/WT_1$ [-], the speed–up inefficiency which essentially compares the actual CPU time due to the simultaneous utilization of N computational nodes, subdivided between pre–processing and calculation time ($CT_N = CT_N^P + CT_N^C$), and the wall clock time due to single–node calculations (WT_1).

A reference test case has been reported for benchmarking. This makes use of a porous medium defined by a physical grid of 33 x 33 elementary cells, which can be available or not for the fluid flow according to the porosity considered (50 %). The reported test is based on a single–class granulometry, which means that all the obstructions are characterized by the same size.

In order to produce mesh independent results, the computational grid size was chosen to be 8 times smaller than that of the physical one. For this reason, the number of computational cells increased (264 x 264) but only the cells available for the fluid flow must be considered (264 x 264 x 0.5 = 34,848). Since the discrete lattice considered is characterized by 9 microscopic velocities, the rough number of unknowns for both cases is 313,632 (order 10^5), which is enough for benchmarking purposes.

In the following calculations, an increasing number of nodes was considered (1, 4, 8, 16, 32, 48) in order to analyze the speed–up efficiency. The computational domain was automatically split by the code among the available nodes during the pre–processing step. The split parallel solution for the test reference case, when 32 computational nodes were used, is reported in Fig. 1. The numerical results for the scaling analysis are reported in Table 1. Finally, the calculated inefficiencies (reciprocal of the efficiency) are shown in Fig. 2.

[1] A 2200 node cluster will be operational shortly and available for use with our code.

Table 1. Scaling analysis for the test reference case.

Number of Nodes	Time due to Pre-Processing	Time due to Calculation	Total Time
[-]	[s]	[s]	[s]
1	407	1198	1605
4	22	403	425
8	7	195	202
16	2	114	116
32	1	81	82
48	<1	78	79

The preliminary results are positive and a significant speed–up occurs, at least for a limited number of nodes ($N \le 16$). For a high number of nodes $N > 16$, the parallelization reduces its effectiveness. This is essentially due to unbalanced decomposition. Let us consider again the Fig. 1, which shows the computational cells where the equations are solved. According to the considered porosity (50 %), the number of computational cells roughly equals the number of the solid cells where the equations are not solved. When the computational domain is decomposed among cluster nodes, this balance is no more satisfied for every node. For example, the bordered node subdomain in Fig. 1 involves only few computational cells and, at a generic time step, it will complete its work much faster than other overloaded nodes. Hence the code still needs some optimization. On the other hand, at any rate the pre–processing receives a great benefit from parallelization. In particular, finding for each cell the labels of neighboring cells requires a computational time, which exponentially decreases when smaller domains are considered. The pre–processing is an additional step which simplifies the computational step on complex topologies and the parallel results confirm that it is a winning strategy for this problem.

In actual fact, the current parallel version of the code needs better strategies for domain decomposition. The test reference case is enough to understand that this issue is particularly critical for a randomly generated porous medium. In particular the elementary partitioning strategy shows its limits and can in the end reduce the effectiveness of parallelization. Some promising ideas are optimized rectilinear partitioning and orthogonal recursive bisection [47, 48]. In the first case, the grid is split into rectilinear-shaped subdomains such that the workload is balanced. In the other case, orthogonal recursive bisection is a partitioning technique which subdivides the computational domain into equal parts of work by successively subdividing along orthogonal coordinate

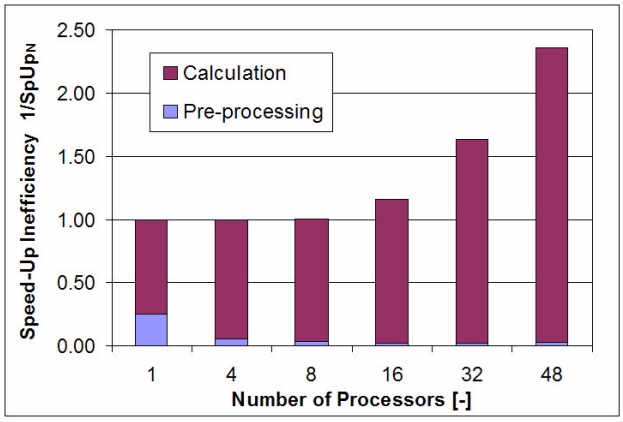

Figure 2. Speed–up inefficiency for the test reference case.

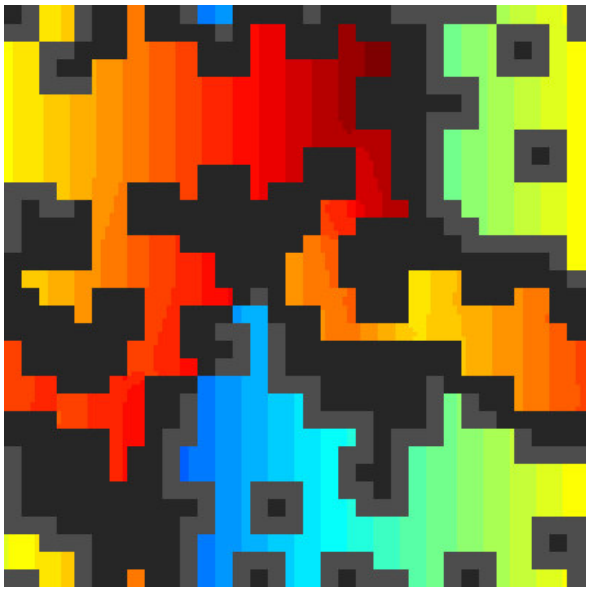

Figure 3. Oxygen concentration without chemical reactions.

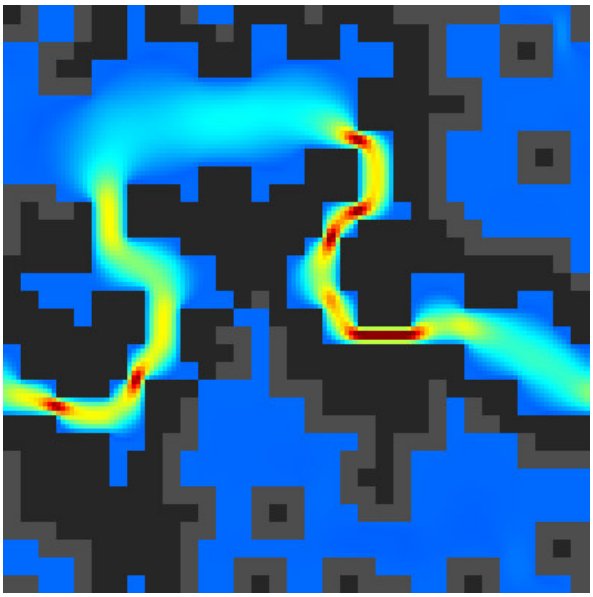

Figure 4. Velocity contours without chemical reactions.

Figure 5. Oxygen concentration with chemical reactions due to the maximum current density.

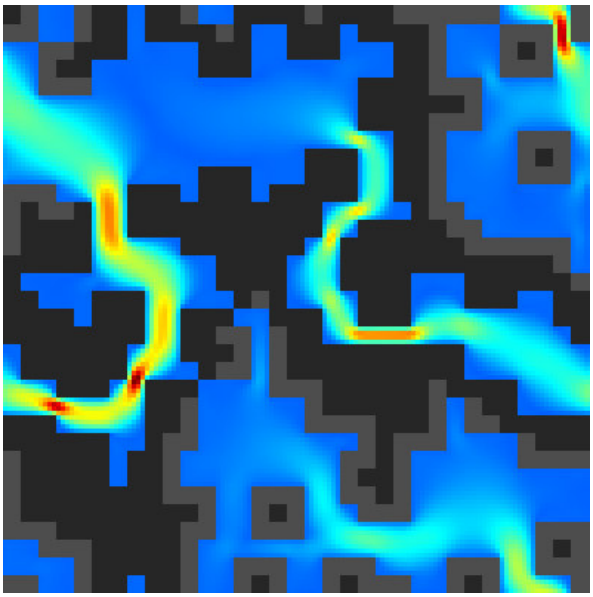

Figure 6. Velocity contours with chemical reactions due to the maximum current density.

directions [48]. This second strategy is currently under investigation in order to implement it in the numerical code.

PRELIMINARY RESULTS AND CONCLUSIONS

Some numerical results are reported here in order to illustrate the capabilities of the numerical code developed. These results are qualitative and must be considered preliminary. The most important limiting factor with regards to these calculations is the fact that they are two–dimensional and for this reason are not suitable for properly matching the microscopic topology of a practical cathode catalyst layer. The extension of the parallel code in order to include three–dimensional geometries is currently under development.

The Figs. 3–6 show the oxygen concentration and the velocity contours in an idealized cathode catalyst layer of a PEM fuel cell. These numerical results are focused on highlighting the effects of the electrochemical reactions at the three–phase boundaries on the microscopic hydrodynamics.

Now, even though the computational domain is ideally two–dimensional, some care has been applied for reproducing in the numerical simulations the same ratio between the active surface and the catalyst layer volume, which is used in the Butler–Volmer equation [49]. In Figs. 3–6, the black obstructions are simply hydrodynamic obstacles, while the dark gray obstructions represent the active sites because they realize the three–phase boundary condition where the reaction can take place. At these active sites, the depletion of oxygen and consequently the production of water proceeds according to the operating current density. Oxygen

depletion and water production can be described by the following expressions,

$$S_{O_2} = -\frac{j M_{O_2}}{4FL_{CL}} < 0\,, \tag{33}$$

$$S_{H_2O} = \frac{j M_{H_2O}}{2FL_{CL}} > 0\,, \tag{34}$$

which are proper source terms with respect to their respective species equations. Both of the previous source terms are tied to the current density associated with a given operating condition. This current density can be easily calculated via the Butler–Volmer equation, namely,

$$j = Aj_{ex}\left(\frac{C_k}{C_{k0}}\right)^{\beta_k}\left[e^{\frac{\gamma_a F\phi_{act}}{RT}} - e^{\frac{\gamma_c F\phi_{act}}{RT}}\right]. \tag{35}$$

Even though the reported results are preliminary, they allow not to qualitatively investigate how the electrochemical reaction affects the hydrodynamics inside the porous cathode catalyst layer at the microscopic level. In the reported example, the concentration gradient induces a net average flow to the right. On the other hand, the active sites are mainly located so as to induce a net suction flow rate to the left; and, for this reason, the electrochemical reaction tends to reverse the direction of the microscopic flow in order to feed the reaction itself. This example is enough to highlight that the hydrodynamics and, consequently, the macroscopic parameters used to characterize this phenomenon can not leave the electrochemical reaction out of the consideration. For this reason, the usual practice of separately investigating the hydrodynamics and electrochemistry seems somehow artificial and far from what actually happens microscopically.

The present work has dealt with the extension of a mesoscopic model for single species fluid flow in porous media to one which describes reactive gas mixtures. It was then applied to a portion of a PEMFC cathode catalyst layer, showing the model's ability to describe oxygen depletion and water production in the presence of three–phase boundary layers (gas phase, polymer, and solid fractions).

Increasing computational needs due to both three–dimensional descriptions and multi–physics models suggest that one must consider large parallel computing. The code parallelization which was done here confirms the LBMs fame with respect to scalability and performance increases. Tests performed on the Virginia Tech cluster facility has demonstrated the feasibility of simulating flow in two–dimensional domains, thus, making it possible to simulate reacting fluid flow in entire fuel cell electrodes. Some evidence exists to the effect that these results can be fruitfully extended to three–dimensional simulations too.

Acknowledgments

The authors would like to acknowledge Prof. Michele Calì for creating the conditions for the development of the present work.

Nomenclature

A : geometrical area
c : lattice speed
C : molar concentration
D : number of spatial dimensions
d : discrete effect factor
e : specific internal energy
f : continuous single particle distribution function
F : Faraday's constant
g : acceleration due to an external field
j : electric current density
k : kinetic forcing term
L : length
m : single particle mass
M : molar mass
Q : collisional operator
R : universal gas constant
S : source / sink term
T : temperature
t : time
u : macroscopic velocity
v : microscopic velocity
w : diffusion velocity
α : interpolation factor
β : kinetics exponent
δ : discrete step
ε : coupling strength
γ : transfer coefficient
ϕ : voltage loss
φ : discrete single particle distribution function
λ : Hamel function
ν : kinetic viscosity
ρ : density
τ : collision time
Ω : control volume
ω : dimensionless collision frequency
ζ : coefficient of quadrature

Subscripts and superscripts

a : generic species
b : generic species
act : activation
CL : catalyst layer
e : equilibrium
k : chemical species
m : mixture
0 : reference value
α : interpolated value
σ : generic species
$\oplus$: modified value
Θ : pre–streamed value

REFERENCES

[1] Bernardi, D. and Verbrugge, M., 1991,"Mathematical Model of a Gas Electrode Bonded to a Polymer Electrolyte", American Institute of Chemical Engineers Journal, Vol. 37, pp. 1151-1163.

[2] Bernardi, D. and Verbrugge, M., 1992,"A Mathematical Model of the Solid-Polymer-Electrolyte Fuel Cell", Journal of the Electrochemical Society, Vol. 139, pp. 2477-2490.

[3] Springer, T., Zawodinski, T. and Gottesfeld, S., 1991, "Polymer Electrolyte Fuel Cell Model", Journal of the Electrochemical Society, Vol. 138, pp. 2334 -2341.

[4] Springer, T., Wilson, M. and Gottesfeld, S., 1993, "Modeling and Experimental Diagnostics in Polymer Electrolyte Fuel Cells", Journal of the Electrochemical Society, Vol. 140, pp. 3513-3526.

[5] Fuller, T. and Newman, J., 1993, "Water and Thermal Management in Solid-Polymer-Electrolyte Fuel Cells, Journal of the Electrochemical Society, Vol. 140, pp. 1218-1225.
[6] Nguyen, T. and White, R., 1993, "A Water and Heat Management Model for Proton-Exchange-Membrane Fuel Cells", Journal of the Electrochemical Society, Vol. 140, pp. 2178-2186.
[7] Gurau, V., Liu, H. and Kakac, S., 1998, "Two-dimensional Model for Proton Exchange Membrane Fuel Cells", American Institute of Chemical Engineers Journal, Vol. 44, pp. 2410-2422.
[8] Yi, J. and Nguyen, T., 1998, "An Along-the-Channel Model for Proton Exchange Membrane Fuel Cells", Journal of the Electrochemical Society, Vol. 145, pp. 1149-1159.
[9] Yi, J. and Nguyen, T., 1999, "Multi-Component Transport in the Porous Electrodes of PEM Fuel Cells with Interdigitated Gas Distributors,", Journal of the Electrochemical Society, Vol. 146, pp. 38-45.
[10] Gu, W., Wang, Y. and Liaw, B., 1997, "Numerical Modeling of Coupled Electrochemical and Transport Processes in Lead-Acid Batteries," Journal of the Electrochemical Society, Vol.144, pp.2053-2061.
[11] Wang, C., Wang, Z. and Pan, Y.,1999, "Two-phase Transport in Proton Exchange Membrane Fuel Cells", in Proceedings of the International Mechanical Engineering Congress & Exhibits, Nashville, USA.
[12] Um, S., Wang, C. and Chen, K., 2000, "Computational Fluid Dynamics Modeling of Proton Exchange Membrane Fuel Cells", Journal of Electrochemical Society, Vol.147, pp.4485-4493.
[13] Wood, D., Yi, J. and Nguyen, T., 1998, "Effect of Direct Liquid Water Injection and Interdigitated Flow Field on the Performance of Proton Exchange Membrane Fuel Cells", Electrochimica Acta, Vol. 43, No. 24, pp.3795-3809
[14] Liu, H. and Zhou, T., 2001, "Numerical Simulation of Performance of PEM Fuel Cells", Proceedings of the 2nd International Conference on Computational Heat and Mass Transfer, Rio de Janeiro, Brasil.
[15] Berning, T., Lu, D. and Djilali, N., 2002, "Three-dimensional Computational Analysis of Transport Phenomena in a PEM Fuel Cell," Journal of Power Sources, Vol. 106, p.284-294.
[16] Siegel, N.P., Ellis, M.W., Nelson, D.J., von Spakovsky, M.R., 2004, "A Two-Dimensional Computational Model of a PEMFC with Liquid Water Transport," Journal of Power Sources, vol. 128, issue 2, pp. 173-184.
[17] Siegel, N.P., Ellis, M.W., Nelson, D.J., von Spakovsky, M.R., 2003, "Single Domain PEMFC Model Based on Agglomerate Catalyst Geometry," Journal of Power Sources, vol. 115/1, pp. 81 - 89.
[18] P. Asinari, M. Coppo, 2004, "Influence of Porous Electrode Structure on PEM Fuel Cells Design and Performance", Proceedings of the 2nd International Conference on Fuel Cell Science, Engineering and Technology, ASME, Rochester N.Y..
[19] D. H. Rothman, 1988, Geophysics, Vol. 53, p. 509.
[20] J. Bernsdorf, M. Schafer, F. Durst, 1999, International Journal of Numerical Methods in Fluids, Vol. 29, p. 251.
[21] J. Bernsdorf, G. Brenner, F. Durst, 2000, "Numerical analysis of the pressure drop in porous media flow with lattice Boltzmann (BGK) automata", Computer Physics Communications, Vol. 129, p. 246-255.
[22] S. Succi, R. Benzi, F. Higuera, 1991, "The lattice-Boltzmann equation: a new tool for computational fluid dynamics", Lattice Gas Methods: Theory, Applications and Hardware, edited by G. Doolen (Elsevier, Amsterdam), reprinted from Physica D, Vol. 47, p. 219.
[23] S. Chen, G. D. Doolen, 1998, "Lattice Boltzmann method for fluid flow", Annual Review of Fluid Mechanics, Vol. 30, p. 329-338.
[24] B. Manz, L.F. Gladden, P.B. Warren, 1999, AIChE. Journal, Vol. 45, pp. 1845.
[25] Th. Zeiser, P. Lammers, E. Klemm, Y.W. Li, J. Bernsdorf, G. Brenner, 2001, Chemical Engineering Science, Vol. 56, pp. 1697.
[26] E.G. Flekkoy, 1993, Physics Review E, Vol. 47, pp. 4247.
[27] X. Shan, G. Doolen, 1995, Journal of Statistical Physics, Vol. 81, pp. 379.
[28] V. Sofonea, R.F. Sekerka, 2001, Physica A, Vol. 299, pp. 494.
[29] Z. Guo, T.S. Zhao, 2003, Physics Review E, Vol. 68, N. 035302.
[30] L.-S. Luo, S.S. Girimaji, 2003, Physics Review E, Vol. 67, N. 036302.
[31] K. Xu, 1997, Journal of Computational Physics, Vol. 134, pp. 122.
[32] K. Xu, 2000, Journal of Computational Physics, Vol. 163, pp. 349.
[33] J.H. Ferziger, H.G. Kaper, 1972, "Mathematical Theory of Transport Processes in Gases", North-Holland, Amsterdam.
[34] S. Chapman, T.G. Cowling, 1970, "The Mathematical Theory of Non-Uniform Gases", Cambridge University Press, Cambridge.
[35] S. Harris, 1971, "An Introduction to the Theory of the Boltzmann Equation", Holt, Rinehart and Winston, New York.
[36] B.B. Hamel, 1963, Ph.D. dissertation, Princeton University.
[37] B.B. Hamel, 1965, Physics of Fluids, Vol. 8, pp. 418.
[38] B.B. Hamel, 1966, Physics of Fluids, Vol. 9, pp. 12.
[39] P. Asinari, 2004, "Viscous coupling based lattice Boltzmann model for binary mixtures", submitted to Physics of Fluids.
[40] C. Cercignani, 1975, "Theory and applications of the Boltzmann equation", Scottish Academic Press, Edinburgh and London, UK.
[41] T. Abe, 1997, "Derivation of the lattice Boltzmann method by means of the discrete ordinate method for the Boltzmann equation", Journal of Computational Physics, Vol. 131, p. 241.
[42] Y. H. Qian, D. D'Humieres, P. Lallemand, 1992, "Lattice BGK Models for Navier-Stokes Equations", Europhysics Letters, Vol. 17, p. 479-484.
[43] X. He, X. Shan, G. D. Doolen, 1998, "A discrete Boltzmann equation model for non-ideal gasses", Physical Review E, Vol. 57, R13.
[44] Q. Zou, X. He, 1997, "On pressure and velocity boundary conditions for the lattice Boltzmann BGK model", Physics of Fluids, Vol. 9, p. 1591-1598.
[45] R. S. Maier, R. S. Bernard, D. W. Grunau, 1996, "Boundary conditions for the lattice Boltzmann method", Physics of Fluids, Vol. 8, p. 1788-1801.
[46] N. MacDonald, E. Minty, T. Harding, S. Brown, "Writing Message-Passing Parallel Programs with MPI", Edinburgh Parallel Computing Centre, The University of Edinburgh.
[47] V. Kumar, A. Grama, A. Gupta, G. Karypis, 1994, "Parallel Computing", Benjamin/Cummings, California.
[48] C. Pan, J. F. Prins, C. T. Miller, 2004, "A high–performance lattice Boltzmann implementation to model flow in porous media", Computer Physics Communications, Vol. 158, pp. 89-105.
[49] Larminie, J. and Dicks, A., 2000, "Fuel Cell Systems Explained" John Wiley and Sons Ltd., ISBN 0-471-49026-1.